Am J Transl Res 2023;15(2):1026-1040
www.ajtr.org /ISSN:1943-8141/AJTR0146321

Original Article

Long noncoding RNA SPRY4-IT1 acts as a miR-101-5p sponge to promote gastrointestinal stromal tumor progression by inhibiting ZEB1

Chen Huang[1], Ming Wang[1], Wen-Yi Zhao[1], Yan-Ying Shen[2], Chun Zhuang[1], Bo Ni[1], Lin-Xi Yang[1], Lu Lu[1], Xiao-Qi Li[1], Lin Tu[1*], Hui Cao[1*]

[1]Department of Gastrointestinal Surgery, Renji Hospital, School of Medicine, Shanghai Jiao Tong University, Shanghai, P. R. China; [2]Department of Pathology, Renji Hospital, School of Medicine, Shanghai Jiao Tong University, Shanghai, P. R. China. [*]Equal contributors.

Received September 4, 2022; Accepted December 20, 2022; Epub February 15, 2023; Published February 28, 2023

Abstract: Objectives: Research on long noncoding RNAs (lncRNAs) has been conducted in different areas of oncology. Currently, the biological significance of lncRNAs and their regulatory features in gastrointestinal stromal tumors (GIST) remain largely unknown. We have previously identified SPRY4-IT1 overexpression in GIST through lncRNA sequencing of GIST tissues. Coincidentally, SPRY4-IT1 is an intron of the SPRY4 gene, and SPRY4 is specifically highly expressed in GIST. Thus the aim of the present study was to investigate the role of lncRNA SPRY4-IT1 in GIST pathogenesis. Methods: Herein, we screened for SPRY4-IT1 and analyzed its possible phenotypes using Gene set enrichment analysis (GSEA). The phenotypes of GIST were verified using CCK-8, colony formation, and wound-healing assays. The ceRNA mechanism was determined by the location of lncRNA SPRY4-IT1, and its relationship to the Ago2 protein. The SPRY4-IT1/miR-101-5p/ZEB1 axis was predicted using online software and sequencing. Luciferase and pull-down assays were performed for verification. Pathway-associated and phenotype-associated proteins were detected by western blotting. Results: Sequencing analysis revealed 117 differentially expressed lncRNAs in GIST and normal gastric tissue samples. Accordingly, SPRY4-IT1 was screened out and its phenotype was predicted by GSEA. Mechanistically, SPRY4-IT1 was identified as a competing endogenous RNA (ceRNA) that downregulated miR-101-5p and upregulated ZEB1, which activated extracellular signal-regulated kinase (ERK) signaling to stimulate GIST proliferation, invasion, and epithelial-mesenchymal transition. Although this effect was regulated by a negative feedback loop through SPRY4, it was still controlled by SPRY4-IT1. Conclusions: In GIST, we revealed a ceRNA mechanism by which SPRY4-IT1 modulates ZEB1 by sponging miR-101-5p, eventually driving tumor cell proliferation, migration, and epithelial-mesenchymal transition (EMT).

Keywords: SPRY4, SPRY4-IT1, ERK, ZEB1, GIST, miR-101-5p

Introduction

Gastrointestinal stromal tumors (GIST) are the most common sarcoma [1-3], and "risk assessment" is the most important prognostic factor for GIST [3]. During genome transcription, hundreds of long noncoding RNAs (lncRNAs), with lengths greater than 200 nucleotides, are produced [4, 5]. LncRNAs have been studied in numerous subdivided areas of cellular functions, including cell proliferation, cell metabolism, metastasis, and epithelial-mesenchymal transition (EMT) [6]. The mechanisms of lncRNAs in cells are diverse, and among them, competing endogenous RNA (ceRNA), mechanism of RNA interaction, is particularly important. This mechanism involves lncRNAs acting as miRNA sponges that competitively bind miRNAs to form an RNA-induced silencing complex (RISC), which in turn weakens the inhibition of mRNA protein synthesis by miRNAs binding to target genes, ultimately increasing protein expression [7-9]. SPRY4-IT1 (HH17, SPRIGHTLY; HGNC, 42394; NCBI Entrez Gene, 100642175; OMIM®, 617617; GenBank Accession ID, AK024556) is an intron within SPRY4 [10, 11]. Recent studies have shown that in various cancers, for example, gastric

cancer and hepatocellular carcinoma [12-14], SPRY4-IT1 is upregulated and is likely involved in tumor proliferation, tumor metastasis, and resistance to antineoplastic agents. In the present study, we evaluated the effect of SPRY4-IT1 expression on the phenotype of GIST cells. SPRY4 is commonly thought to inhibit the MAPK (RAS-Raf-MEK1/2-ERK1/2) signaling pathway [15-17]. The MAPK signaling pathway contributes to more than 39% of all human tumor-causing effects [18]. The MAPK/extracellular signal-regulated kinase (ERK) signaling pathway is a classical signaling pathway that has a major impact on cellular biological activities. Excessive activation of ERK often leads to malignant tumor progression. ERK1 and ERK2 regulate cellular signaling under normal and pathological conditions, and they are evolutionarily conserved.

Materials and methods

Ethics statement

Six pairs of GIST and normal gastric tissue samples were collected from patients admitted to the Renji Hospital. The study design and sampling process were approved by the Ethics Committee of Renji Hospital, and all patients provided informed consent for the use of their clinical samples. All experiments were performed in accordance with the Ethics Committee of Renji Hospital guidelines and regulations. The ethical approval number was KY2020-129.

Cell culture

The cell line GIST-T1 (RRID: CVCL_S983) was obtained from Cosmo Bio, while the cell line GIST-430 (RRID: CVCL_7040) was provided by Prof. Jonathan Fletcher (Brigham and Women's Hospital). GIST-430 and GIST-T1 cells were cultured in IMDM supplemented with 10% fetal bovine serum and 1% antibiotics, and the culture environment was 37°C under a 5% CO_2 atmosphere. Culture-based experiments were performed using Biohazard safety equipment, and mycoplasma was detected in the cell lines.

Transcriptome sequencing

Total RNA was first extracted from GIST and normal tissue samples and RNA integrity was verified. The lncRNA expression profiles of the samples were analyzed using RNAiso (Takara), an Agilent 2100 Bioanalyzer, and the ArrayStar Human LncRNA Array 2.0. Differential expression of lncRNA was defined as a fold-change value of > 2.0 at $P < 0.05$, between GIST and normal tissue samples.

RT-qPCR

Total RNA was extracted using TRIzol reagent (Takara), followed by reverse transcription to get cDNA using a High-Capacity cDNA Reverse Transcription Kit (Takara). SYBR Green Master Mix (Takara), cDNA, and primers (Table S1) were mixed and detected by RT-qPCR. Data were analyzed with the $2^{-\Delta\Delta Ct}$ method. 18S rRNA was used as an internal reference. Each sample was processed in triplicate.

RNA immunoprecipitation (RIP)

A Magna RIP kit (Millipore, Bedford, MA) was used according to the manufacturer's instructions. At 24 h after transfection, 2×10^7 cells were harvested for RIP experiments using an anti-Ago2 antibody (Millipore). The co-precipitated RNAs were then extracted and detected using RT-qPCR. The immunoprecipitated RNA data were analyzed using the $2^{-\Delta\Delta Ct}$ method. The primers in the RISC for detecting SPRY4-IT1 are listed in Table S1. Each sample was processed in triplicate.

Gene set enrichment analysis (GSEA)

To explore the signatures of SPRY4-IT1, GSEA software (GSEA v4.1.0 for Windows, RRID: SCR_003199) was utilized to perform a comparative analysis between high (higher 50%, n = 3) and low (lower 50%, n = 3) expression groups based on SPRY4-IT1 expression from our own dataset. The normalized enrichment score indicated the size and degree of overrepresentation (P value < 0.05, FDR ≤ 0.25).

LncLocator prediction

To determine the subcellular localization of SPRY4-IT1, lncLocator (http://www.csbio.sjtu.edu.cn/cgi-bin/lncLocator.py) was used by filling in the input sequence.

Gene expression profiling interactive analysis (GEPIA)

GEPIA (http://gepia.cancer-pku.cn/index.html, RRID: SCR_018294) was run to identify the cor-

relation between SPRY4-IT1 and SPRY4. Pearson's coefficient was selected under "Correlation Coefficient", and stomach, esophagus-gastroesophageal junction, colon-sigmoid, and colon-transverse were selected under "Used Expression Datasets".

Generation of transiently transfected and stably transfected cell lines

Lenti-CMV-H_SPRY4-IT1-PGK-Puro, lenti-CMV-H_ZEB1-PGK-Puro, lenti-CMV-H_SPRY4-PGK-Puro, and lenti-CMV-H_RAF1-PGK-Puro were purchased from Genomeditech (Shanghai). Stably transfected cells were selected with puromycin (1 μg/mL) to be retained and thus be selected. The efficiency of transfection was verified using RT-qPCR. The miR-101-5p mimics (GenePharma, Shanghai), inhibitor (GenePharma, Shanghai), and negative controls (GenePharma, Shanghai) are shown in Table S2. Cells were first transfected with siRNA using GP-transfect-Mate (GenePharma, Shanghai) for 48 h and then harvested for assays. siRNA-SPRY4-IT1 (GenePharma, Shanghai), siRNA-ZEB1 (GenePharma, Shanghai), siRNA-SPRY4 (GenePharma, Shanghai), and siRNA-RAF1 (GenePharma, Shanghai) are shown in Table S2.

CCK-8 and colony formation assays

GIST-T1/430 cells were seeded into 96-well plates (1×10^4 cells/well) to assess their proliferative ability. Subsequently, the absorbance at 450 nm was measured every 24 hours using the Cell Counting Kit-8 (Absin, Shanghai). The data from 6 consecutive days were collected, and each sample was processed in quintuplicate.

The tumor cell suspension was diluted to 2×10^3 cells/mL, seeded into 6-well plates, and incubated at 37°C in a 5% CO_2 atmosphere for 14 days. After discarding the medium, cells were washed, fixed in 4% paraformaldehyde, and stained with crystalline violet (0.2%) for 10 minutes. Cells were observed, and each sample was processed in triplicate.

Wound healing assay

Tumor cells were inoculated into 6-well plates and cultured to a subconfluent state. The original medium was then discarded, and the cells were starved for 24 hours using a serum-free medium. Artificial wounds were induced using a pipette tip, and images were captured using a microscope at 0, 24 and 48 h. Each sample was processed in triplicate.

Transwell migration assay

Tumor cells were seeded into 8-μm well Transwell chambers (Corning). The upper chamber was filled with 200 μL of serum-free medium containing 2×10^4 tumor cells, while the lower chamber was filled with 600 μL of complete medium (10% fetal bovine serum). After 48 h, the cells were fixed with formaldehyde and then stained with 0.2% crystalline violet for 10 minutes. Images were acquired using a microscope.

Subcellular fractionation

RNA isolating was performed by the NE-PER™ Reagent (Invitrogen).

Luciferase reporter assay

The mutant SPRY4-IT1 fragment, wild-type SPRY4-IT1 fragment, and the ZEB1 3'-UTR containing the predicted binding sites of miR-101-5p (fragments that need to be predicted whether they can be bound or not) were subcloned into the psiCHECK2 dual-luciferase vector (Promega). The reporter plasmids were cotransfected with miR-101-5p mimics or the negative control into GIST cells. The results were then determined using the Dual-Luciferase Reporter Assay System (Promega) according to the manufacturer's instructions. Each sample was processed in triplicate.

Fluorescence in situ hybridization

After immobilization, the tissue slides were hybridized with the FAM (488)-labeled SPRY4-IT1 fluorescence in situ hybridization (FISH) probe mixture, and the nuclei were stained using DAPI. Images were acquired using a fluorescence microscope (Nikon).

Biotin-labeled miRNA pull-down assay

To identify the target RNAs of miRNAs, biotin-labeled miRNA pull-down assays were performed. Cells were transfected with biotin-labeled miR-101-5p or miR-Ctrl (50 nM) and

harvested after 48 h to prepare lysates. Subsequently, streptavidin-coupled Dynabeads (Invitrogen) were washed and were resuspended in buffer and biotin-labeled miRNA was added for 10 min at 20°C. The coated Dynabeads were isolated using a magnet for 3 minutes followed by three washes. Finally, the RNA was analyzed using RT-qPCR. Each sample was processed in triplicate.

Western blot analysis

Total proteins were extracted from samples using RIPA-Lysate buffer (Biosharp) containing 1 × protease inhibitor (Selleck). Standardized protein concentrations were determined using a BCA Protein Assay Kit (Pierce Biotechnology, USA). Total protein was separated on a 10% SDS-PAGE gel (30 μg/lane) and transferred onto a nitrocellulose membrane. The membranes were blocked with 5% skim milk for 1 h and then incubated overnight at 4°C with the following primary antibodies: anti-SPRY4 (1:1000, Absin, abs153824), anti-ZEB1 (1:1000, Absin, abs136926), anti-RAF1 (1:1000, Absin, abs115036), anti-E-cadherin (1:1000, Absin, abs130068), anti-N-cadherin (1:1000, Absin, abs131133), anti-Snail (1:1000, Absin, abs151371), anti-vimentin (1:1000, Absin, abs131996), anti-t-ERK (1:1000, Cell Signaling Technology, #9102), anti-p-ERK (1:1000, Cell Signaling Technology, #9101), and anti-GAPDH (1:1000, Absin, abs132004). The membrane was then incubated with an HRP-conjugated secondary antibody (1:2000, Absin, abs20002), and the proteins were detected using an ECL reagent solution (Share-Bio, Shanghai). The molecular weight for each protein band was as follows: SPRY4 (33 kDa), ZEB1 (200 kDa), RAF1 (73 kDa), E-cadherin (97 kDa), N-cadherin (100 kDa), vimentin (54 kDa), Snail (29 kDa), t-ERK (43 kDa and 41 kDa), p-ERK (43 kDa and 41 kDa), and GAPDH (37 kDa).

Immunohistochemistry

Tissue samples were dewaxed using xylene and placed in gradient alcohol for rehydration. Antigen repair was performed using a citrate buffer. Samples were incubated with H_2O_2 (0.3%) at 37°C for 20 minutes to inactivate endogenous peroxidases. The samples were then blocked with 10% bovine serum albumin for 1 h and incubated at 4°C with the primary anti-SPRY4 antibody (1:1000, Absin, abs153824) overnight, and the samples were then incubated with the corresponding HRP-conjugated secondary antibody. Finally, SPRY4 was detected using the DAB substrate kit (Cell Signaling Technology). The images were captured using a microscope (Nikon).

Statistical analysis

SPSS 22.0, R (version 4.1.0), and GraphPad 7.0 software were used for statistical analyses. Two-tailed Student's t tests were calculated for the evaluation of differences between groups. Chi-square values were used for correlation analysis. Statistical significance was set at a *P* value < 0.05 (*P < 0.05, **P < 0.01, and ***P < 0.001).

Results

LncRNA SPRY4-IT1 was overexpressed in high-risk GIST

We performed lncRNA sequencing of six pairs of GIST and normal gastric tissues to screen out lncRNAs involved in GIST tumor characteristics. Based on a cutoff value of fold change ≥ 4, we detected 117 differentially expressed lncRNAs (P < 0.01; Figure S1A, S1B). Based on the highest difference, SPRY4-IT1 was the primary focus of the present study (**Figure 1A**; Table S3).

We also evaluated SPRY4-IT1 expression in GIST tissues (23 low-risk samples, 14 intermediate-risk samples, 29 high-risk samples, and 12 metastatic samples) using RT-qPCR, which demonstrated that SPRY4-IT1 was differentially expressed in GIST at different risk levels. In addition, SPRY4-IT1 expression was significantly upregulated in the higher risk GIST tissue samples (**Figure 1B**).

Furthermore, SPRY4-IT1 was remarkably overexpressed in GIST-T1/430 compared to other cell lines (**Figure 1C**).

SPRY4-IT1 promotes GIST proliferation and migration

First, we performed GSEA based on our own dataset to analyze the possible function of SPRY4-IT1 in GIST. The results revealed a remarkable enrichment of high SPRY4-IT1

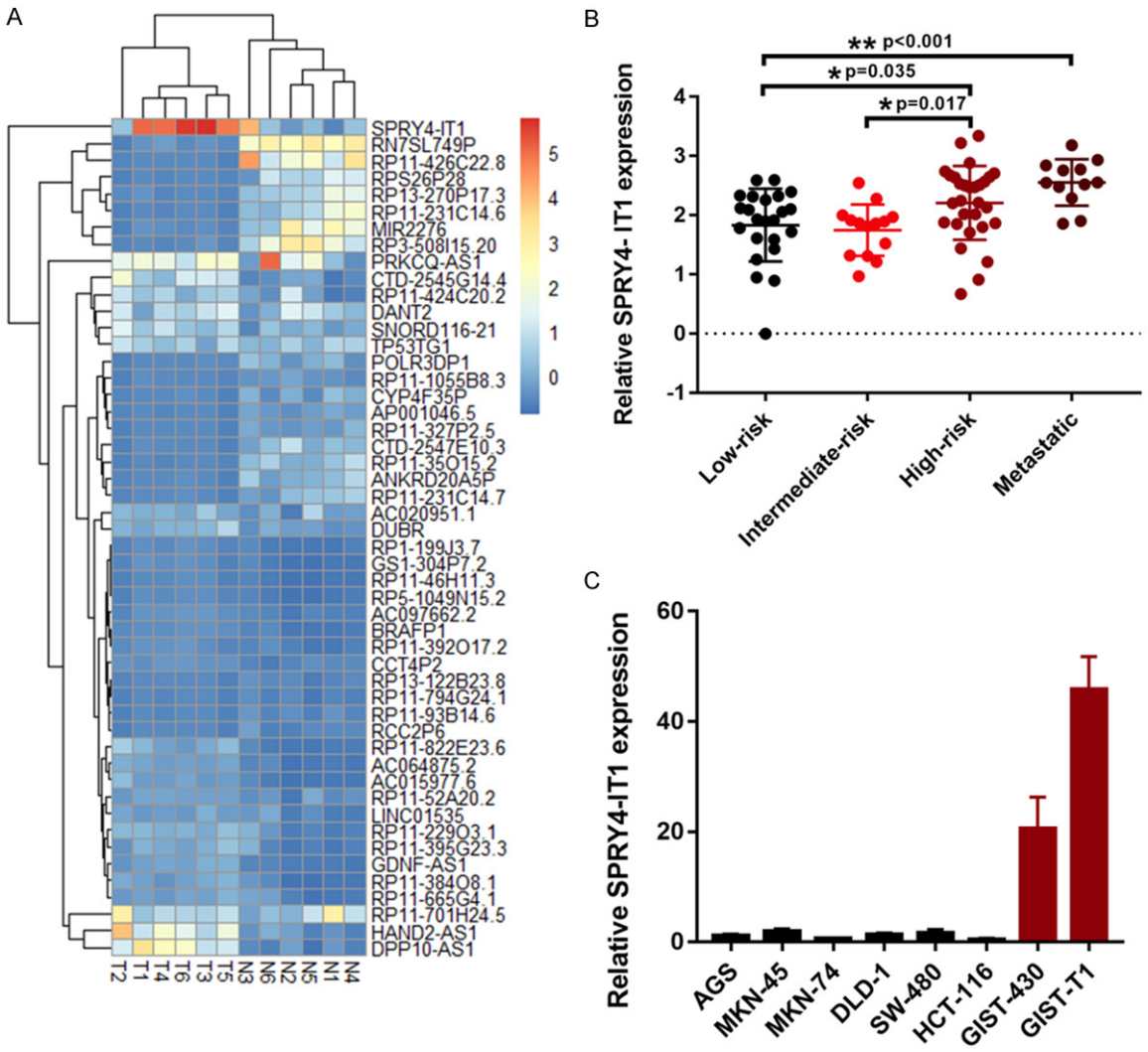

Figure 1. SPRY4-IT1 is overexpressed in high-risk GIST. A. Differentially expressed lncRNAs in six GIST tissues and normal gastric tissues (FC ≥ 2, P < 0.01). B. Relative expression of SPRY4-IT1 in GIST tissues (low-risk n = 23, intermediate-risk n = 14, high-risk n = 29, and metastatic n = 12). C. SPRY4-IT1 expression level in the GIST-T1 cell line, GIST-430 cell line, and some other common cell lines (gastric cancer and colorectal cancer). Data are displayed as the mean ± SD.

expression in genetic datasets in connection with cell proliferation, metastasis, and EMT (**Figure 2A**). To investigate the role of SPRY4-IT1 in the proliferative and metastatic abilities of GIST cells, we transfected GIST-T1/430 cells with two siRNAs to knock down SPRY4-IT1 (siRNA-SPRY4-IT1 #1 and #2) or with a SPRY4-IT1-overexpressing plasmid (Lenti-CMV-H_SPRY4-IT1-PGK-Puro) (**Figure 2B**, **2C**). Proliferation curves and colony formation assays revealed that knocking down SPRY4-IT1 remarkably inhibited the proliferation of GIST, and the opposite phenomenon was noted after SPRY4-IT1 overexpression (**Figure 2D-G**, all P < 0.01). Also, wound healing images and transwell migration assays indicated that SPRY4-IT1 knock down inhibited the GIST cell migration phenotype (Figure S2A-D), whereas SPRY4-IT1 overexpression enhanced the cell migration phenotype (Figure S2E-H). The above results indicated that SPRY4-IT1 works in a pro-tumorigenic manner in GIST.

SPRY4-IT1 acts as a ceRNA and competitively absorbs miR-101-5p

We utilized the lncLocator online software to explore where and how SPRY4-IT1 performs its

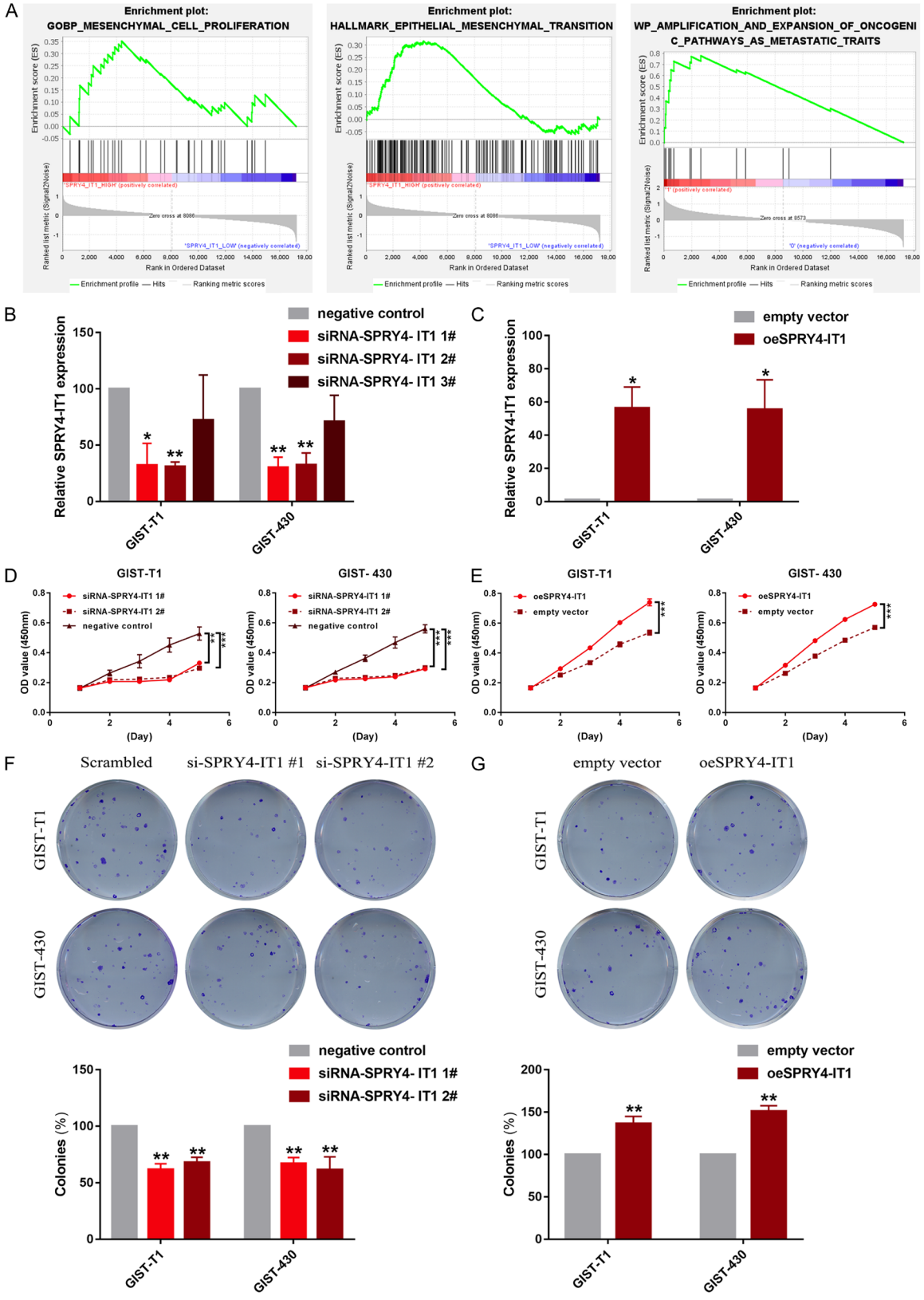

Figure 2. SPRY4-IT1 promotes GIST proliferation and colony formation. (A) Gene set enrichment analysis showed high SPRY4-IT1 expression enriched for proliferation-associated, metastasis-associated, and EMT-associated biological functions. (B, C) Expression of SPRY4-IT1 in GIST-T1/430 transfected with siRNA-SPRY4-IT1s or negative

control (B) and in GIST-T1/430 transfected with Lenti-CMV-H_SPRY4-IT1-PGK-Puro or empty vector (C). (D) Proliferation curves of GIST-T1/430 (siRNA-SPRY4-IT1s or negative control). (E) Proliferation curves of GIST-T1/430 (Lenti-CMV-H_SPRY4-IT1-PGK-Puro or empty vector). (F) Colony formation graphics of GIST-T1/430 (siRNA-SPRY4-IT1s or negative control) [representative images (Up) and quantification (Down)]. (G) Colony formation graphics of GIST-T1/430 (Lenti-CMV-H_SPRY4-IT1-PGK-Puro or empty vector) (representative images [Up] and quantification [Down]). Data are displayed as the mean ± SD. *P < 0.05, **P < 0.01. The experiments were independently repeated at least three times.

biological functions, which predicted SPRY4-IT1 to be located mostly in the cytoplasm (**Figure 3A**). RT-qPCR of nuclear and cytoplasmic SPRY4-IT1 also revealed that this lncRNA was mainly localized in the cytoplasm, which was verified again using FISH in GIST tissue (**Figure 3B**, **3C**, P < 0.05). These results suggested that SPRY4-IT1 plays the role as a competing endogenous RNA (ceRNA). Ago2 was considered the irreplaceable component of the RISC, which participates in translational repression or miRNA-mediated mRNA destabilization. Therefore, we performed RIP and found that endogenous SPRY4-IT1 combined with Ago2-RIPs compared to the IgG-RIP control (**Figure 3D**, P < 0.01). These findings indicated that SPRY4-IT1 functions as a ceRNA.

GIST-T1 cells were subjected to microRNA sequencing and transcriptome sequencing. The cells were divided into overexpression (oe), negative control (nc), and knockdown groups. Between the oe and nc groups, 73 differentially expressed microRNAs were identified (logfc < -1, P < 0.05) (Table S4). Between the si and nc groups, 69 differentially expressed microRNAs were identified (logfc > 1, P < 0.05) (Table S5). The intersection of these two comparisons identified 12 microRNAs (Table S6). The Ago-2-RIP assay revealed that miR-101-5p was the most enriched miRNA (Figure S3). We also found that SPRY4-IT1 was higher in the miRNA overexpression group (**Figure 3E**, **3F**, P < 0.01), which indicated that SPRY4-IT1 and miR-101-5p were in the same RISC. Further, the dual-luciferase reporter assay showed that miR-101-5p's overexpression decreased the activity of the wild-type SPRY4-IT1 reporter but not that of SPRY4-IT1-464Mut (**Figure 3G-I**, P < 0.05). Moreover, SPRY4-IT1 expression was significantly increased in GIST cells transfected with biotin-labeled miR-101-5p in biotin-labeled miRNA pull-down assays (**Figure 3J**, P < 0.01). Furthermore, SPRY4-IT1 knock down significantly increased the expression of miR-101-5p (**Figure 3K**, P < 0.01), and in turn, the overexpression of miR-101-5p remarkably suppressed SPRY4-IT1 expression (**Figure 3L**, P < 0.01). Together, these results indicated that SPRY4-IT1 sponges miR-101-5p.

SPRY4-IT1 functions as a decoy for miR-101-5p to improve ZEB1 expression

To identify genes affected by SPRY4-IT1 sponging miR-101-5p, we run RNAInter (Table S7) and TargetScan (Table S8) to screen target genes of miR-101-5p, which identified an intersection set containing 15 genes (Table S9). In the abovementioned transcriptome sequencing, we identified 126 possible genes in the oe and nc comparison with a filter of logfc > 2 and P < 0.05 (Table S10). In the si and nc comparison, we identified 2034 possible genes with a filter of logfc < -2 and P < 0.05 (Table S11). The intersection between the two comparisons identified three genes (ZEB1, TTLL6, and THBS2). Among these, ZEB1 was the only gene that was present in both the sequencing and predicted results, which indicated that ZEB1 was the only target gene (**Figure 4A**, **4B**, P < 0.01).

To further analyses of ZEB1 expression, we constructed wild-type and mutant ZEB1 3'-UTR reporter plasmids (**Figure 4C**). Overexpression of miR-101-5p inhibited luciferase activity in the wild-type group but did not significantly inhibit the luciferase activity in the mutant group (**Figure 4D**, **4E**). Moreover, miRNA pull-down validated the status of ZEB1 as the target gene (**Figure 4F**, P < 0.01).

The ZEB1 protein-related results showed that both overexpression and knock down of SPRY4-IT1 affected the expression of ZEB1 (**Figure 4G**, **4H**, P < 0.01). GEPIA also detected a strong correlation between SPRY4-IT1 and ZEB1 in GIST. These findings above indicated the existence of a regulatory relationship between SPRY4-IT1 and miR-101-5p (**Figure 4I**, P < 0.01).

Several studies have suggested that ZEB1 promotes oncogenesis by triggering the ERK signaling pathway [19, 20]. So we investigated

A

---------- lncLocator Prediction Result ----------

Subcellular locations	score
Cytoplasm	0.887666282213
Nucleus	0.0334581417202
Ribosome	0.0291770311409
Cytosol	0.0444147758713
Exosome	0.00528376905436

Predicted location
Cytoplasm

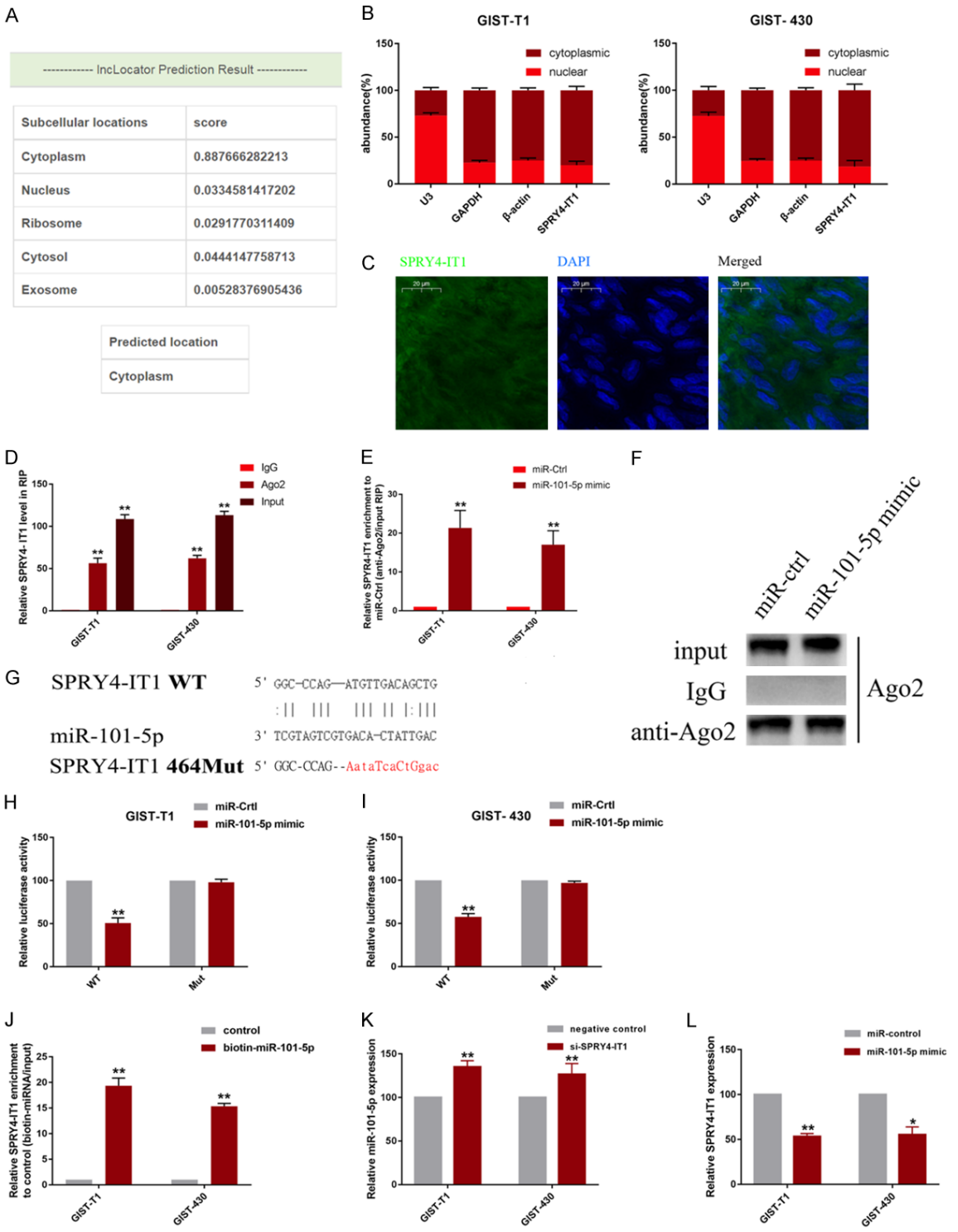

Figure 3. SPRY4-IT1 competitively absorbs miR-101-5p. (A) SPRY4-IT1 located mainly in the cytoplasm predicted by lncLocator: long noncoding RNA subcellular localization predictor. (B) RT-qPCR of SPRY4-IT1 expression in the nucleus and cytoplasm of GIST-T1/430. U3, β-actin, and GAPDH as endogenous controls. (C) Subcellular localization of SPRY4-IT1 (green) in GIST tissue detected using RNA-FISH. (DAPI: blue). (D) Fold enrichment of SPRY4-IT1 in GIST-T1/430. (E, F) Enrichment of SPRY4-IT1 in GIST-T1/430 (miR-101-5p mimic/miR-Ctrl) (E). Detection of Ago2 protein (Ago2 antibody or IgG) using western blotting (F). (G) Binding sites and mutant sequences (red) on SPRY4-IT1 transcript. (H, I) Luciferase assays for GIST-T1 (H) and GIST-430 (I) co-transfected with wild-type or 464Mut SPRY4-IT1 plasmid with miR-101-5p mimic/miR-Ctrl. (J) SPRY4-IT1 pulled down (biotin-miR-101-5p or negative control). (K) Relative levels of miR-101-5p in GIST-T1/430 (siRNA-SPRY4-IT1 #2 or negative control). (L) Relative levels of SPRY4-IT1 in GIST-T1/430 (with miR-101-5p mimic/miR-Ctrl). Data are displayed as the mean ± SD. *P < 0.05, **P < 0.01. The experiments were independently repeated at least three times.

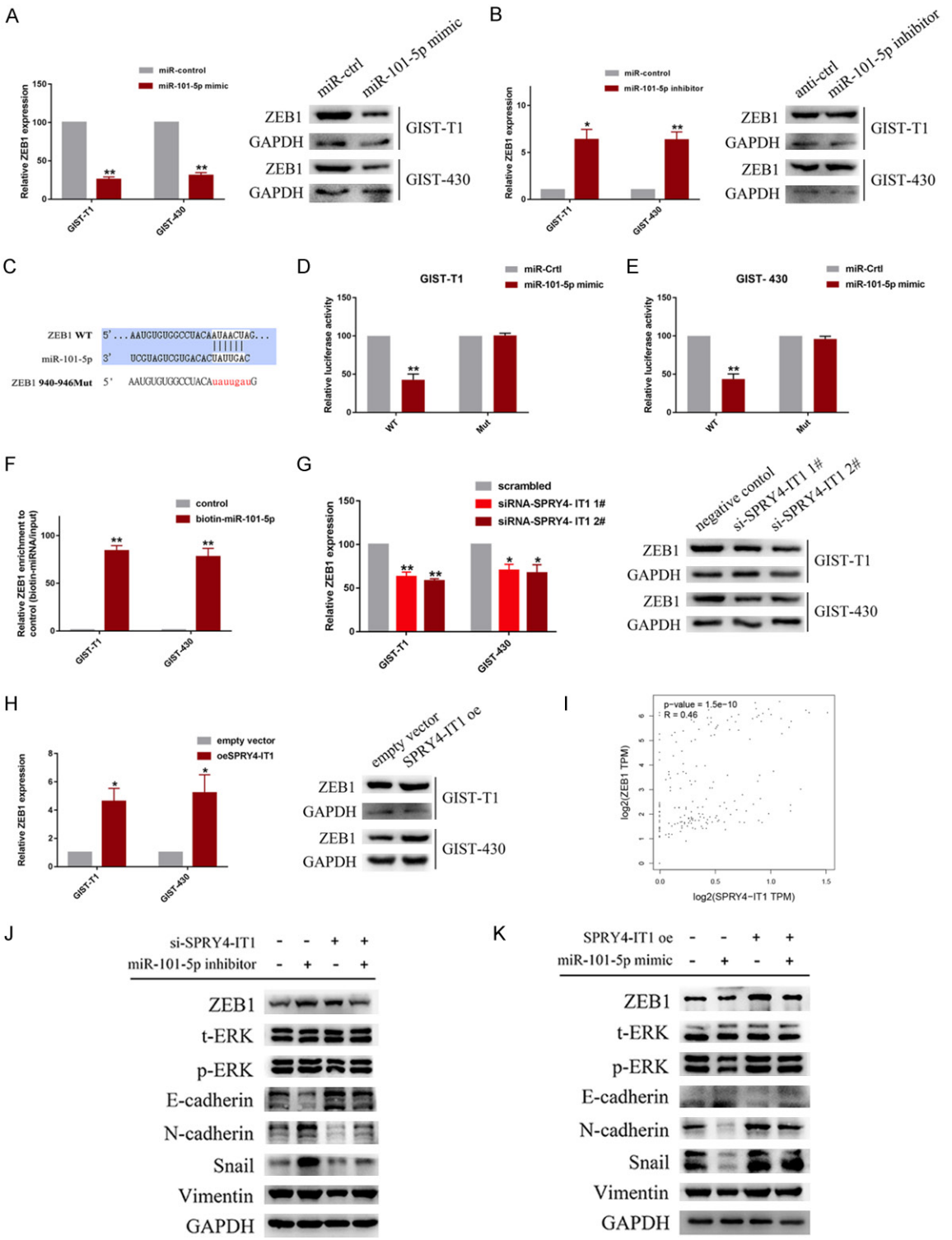

Figure 4. SPRY4-IT1 functions as a decoy for miR-101-5p to increase ZEB1 expression. (A) Relative mRNA levels and protein levels of ZEB1 in GIST-T1/430 (miR-101-5p mimic/miR-Ctrl). (B) Relative mRNA levels and protein levels of ZEB1 in GIST-T1/430 (miR-101-5p inhibitor/anti-Ctrl). (C) Binding sites and mutant sequences (red) on 3'-UTR of ZEB1 transcript. (D, E) Luciferase assays in GIST-T1 (D) and GIST-430 (E) co-transfected wild-type 940-946Mut ZEB1 plasmid with miR-101-5p mimic/miR-Ctrl. (F) ZEB1 pulled down by biotin-labeled miR-101-5p or negative control. (G, H) Relative mRNA levels and protein levels of ZEB1 in GIST-T1/430 (siRNA-SPRY4-IT1s or its negative control) (G), the same as Lenti-CMV-H_SPRY4-IT1-PGK-Puro or its empty vector. (I) GEPIA analysis: SPRY4-IT1 and ZEB1 expression. (J) Western blotting analysis of ZEB1, p-ERK, E-cadherin, N-cadherin, Snail, and Vimentin (co-transfected

with siSPRY4-IT1 #2 or negative control together with miR-101-5p inhibitor). (K) Western blotting analysis of ZEB1, p-ERK, E-cadherin, N-cadherin, Snail, and Vimentin (co-transfected with Lenti-CMV-H_SPRY4-IT1-PGK-Puro or empty vector together with miR-101-5p mimic). Data are displayed as the mean ± SD. *P < 0.05, **P < 0.01. The experiments were independently repeated at least three times.

whether regulation of the SPRY4-IT1-miR-101-5p axis affects the activation of the MAPK pathway. SPRY4-IT1 knock down decreased the levels of ZEB1 protein and phosphorylated ERK (p-ERK), and these effects were partially reversed by co-transfection with miR-101-5p inhibitors partially (**Figure 4J**). In contrast, SPRY4-IT1 overexpression upregulated ZEB1 and p-ERK protein levels, and these effects were partially reversed by co-transfection with miR-101-5p mimics (**Figure 4K**). These findings demonstrated the presence of the SPRY4-IT1-miR-101-5p signaling axis with ZEB1 as the target gene and ERK as the downstream signaling pathway.

ZEB1 regulates SPRY4-IT1-mediated cell proliferation and migration via the ERK signaling pathway

To study the ability of SPRY4-IT1 to influence the ERK signaling pathway by regulating ZEB1, we used GIST-T1/GIST-430 cells with knocking down SPRY4-IT1/overexpression of ZEB1. The results showed that restoration of ZEB1 expression rescued the inhibitory impact of SPRY4-IT1 knock down on GIST cell proliferation, migration, invasion, and EMT (**Figure 5A-I**, P < 0.01). Rescue experiments demonstrated that overexpression of ZEB1 upregulated p-ERK levels, while p-ERK levels were inhibited by SPRY4-IT1 downregulation. However, the knocking down of ZEB1 demonstrated the opposite result (**Figure 5H**, **5I**). Therefore, we concluded that SPRY4-IT1 is a tumor-promoting lncRNA that promotes GIST cell tumor phenotypes according to the SPRY4-IT1-miR-101-5p-ZEB1-ERK signaling pathway (**Figure 5J**).

SPRY4 is overexpressed in high-risk GIST and inhibits GIST cell proliferation and colony formation by inhibiting RAF1

GEPIA identified a strong correlation between SPRY4-IT1 and SPRY4 in GIST (**Figure 6A**). To examine the regulation of the relationship between SPRY4-IT1 and SPRY4, we transfected GIST-T1/430 cells with two siRNAs against SPRY4-IT1 or transfected GIST-T1/430 cells with a SPRY4-IT1 overexpressing plasmid. RT-qPCR revealed that SPRY4 was upregulated after SPRY4-IT1 overexpression, whereas it was downregulated after SPRY4-IT1 knock down (**Figure 6B**). According to the sequencing results, the heatmap showed that SPRY4 was a highly upregulated gene in GIST compared to normal gastric tissue samples (**Figure 6C**). These results were validated in cell lines (by qRT-qPCR) and tumor tissues (by qRT-qPCR and immunohistochemistry) as well as by using online databases (Figure S4). We transfected GIST-T1/430 cells with two siRNAs against SPRY4 (siRNA-SPRY4 #1 and siRNA-SPRY4 #2) or transfected with a SPRY4 overexpressing plasmid (Lenti-CMV-H_SPRY4-PGK-Puro), and the transfection efficiency was confirmed (Figure S5A, S5B). Proliferation curves and colony formation assays showed a significant increase in the proliferation of GIST cells transfected with the si-SPRY4s compared to the negative controls, while the opposite effects were observed after SPRY4 overexpression (**Figure 6D-G**, all P < 0.05). Furthermore, rescue experiments revealed that the overexpression of SPRY4 decreased p-ERK levels, which were increased by RAF1 overexpression, whereas SPRY4 knock down exhibited the opposite effect (**Figure 6H**, **6I**). Finally, we show the mechanism discussed above in the form of a schematic diagram (**Figure 6J**).

Discussion

In the present study, we found that lncRNA SPRY4-IT1 was highly upregulated in GIST tissues compared to normal gastric tissues. SPRY4-IT1 promoted the proliferation, metastasis, and EMT of GIST cells *in vitro* by acting as a ceRNA to sponge miR-101-5p, resulting in ZEB1 gene upregulating. The findings above suggested that lncRNA SPRY4-IT1 plays an oncogenic role in GIST. LncRNAs are being increasingly used as prognostic indicators of tumors [21, 22]. Here, RT-qPCR was used to measure the expression level of SPRY4-IT1 in GIST tissue samples, which confirmed that SPRY4-IT1 was significantly overexpressed in GIST.

By competitively binding to miRNAs, lncRNAs function as ceRNAs, thereby positively modulating the mRNAs of their target genes [23, 24].

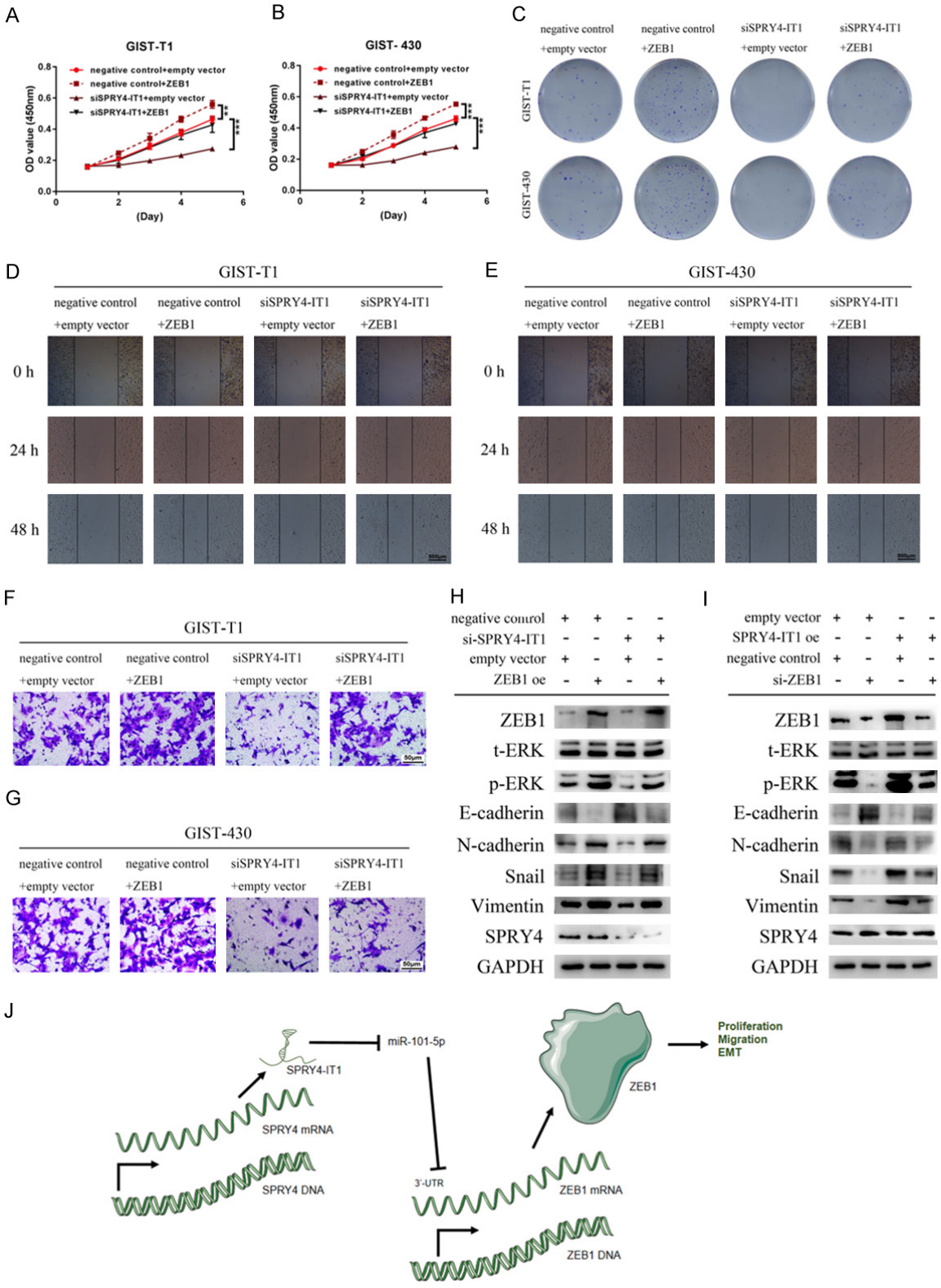

Figure 5. ZEB1 is the target of SPRY4-IT1 for proliferation and migration. (A, B) Proliferation curves of GIST-T1 (A)/430 (B) (co-transfected with siRNA-SPRY4-IT1 #2 or scrambled control and Lenti-CMV-H_SPRY4-IT1-PGK-Puro or empty vector). (C) Colony formation graphics in the abovementioned GIST cells. (D, E) Wound healing assays in the abovementioned GIST cells. (F, G) Transwell migration assays in the abovementioned GIST cells. (H) Western blotting analysis of ZEB1, SPRY4, p-ERK, E-cadherin, N-cadherin, Snail, and Vimentin in GIST cells (co-transfected with siRNA-SPRY4-IT1 #2 or scrambled control together with lenti-CMV-H_ZEB1-PGK-Puro or empty vector). (I) West-

ern blotting analysis of ZEB1, SPRY4, p-ERK, E-cadherin, N-cadherin, Snail, and Vimentin in GIST cells (co-transfected with Lenti-CMV-H_SPRY4-IT1-PGK-Puro or empty vector together with siRNA-ZEB1 or scrambled control). (J) Schematic diagram of SPRY4-IT1 in GIST cell phenotype. Data are displayed as the mean ± SD. *P < 0.05, **P < 0.01, ***P < 0.001. The experiments were independently repeated at least three times.

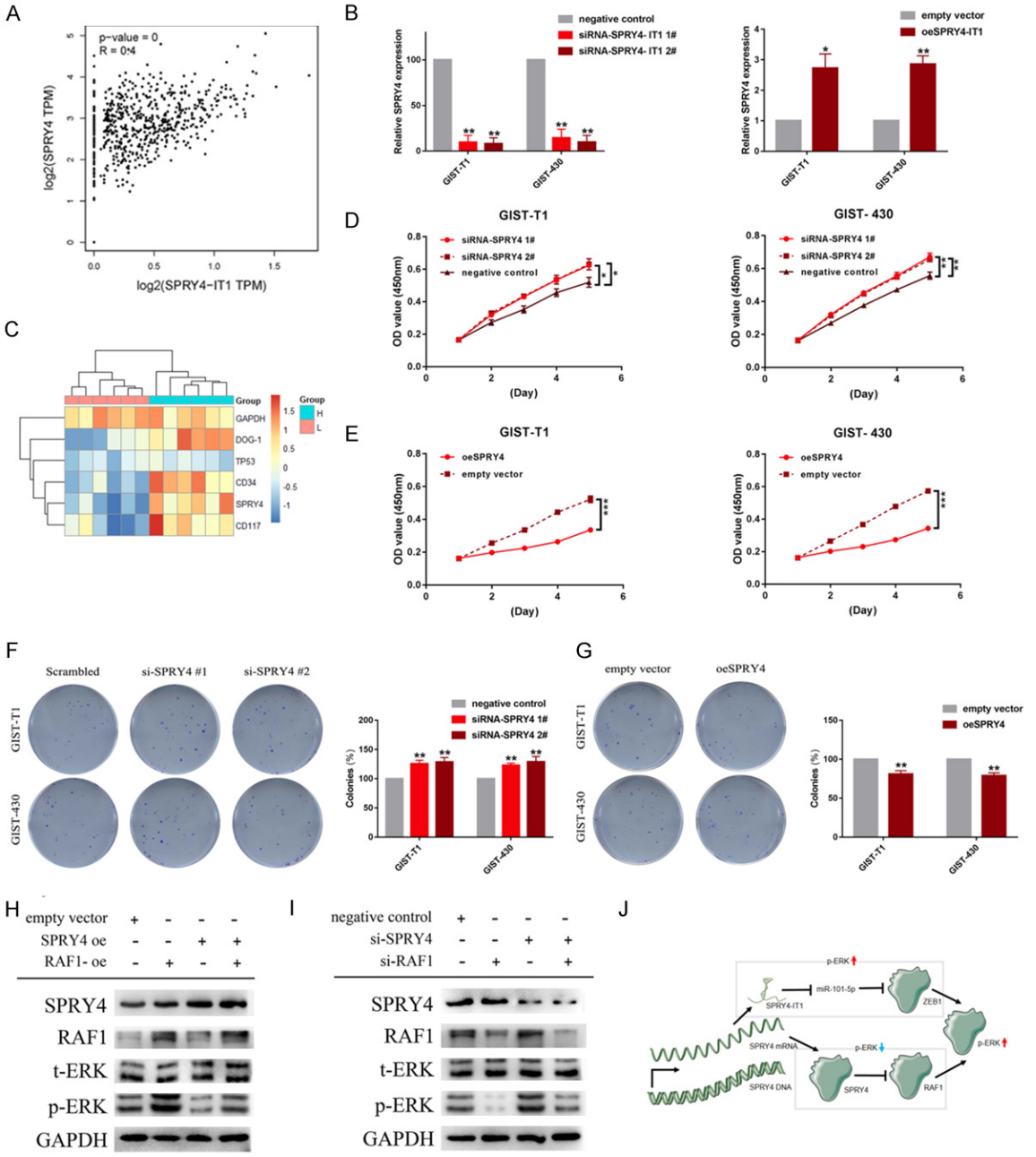

Figure 6. SPRY4 is overexpressed in high-risk GIST and inhibit s GIST cell proliferation and colony formation by inhibiting RAF1. A. GEPIA analysis: SPRY4 and SPRY4-IT1 expression. B. Expression of SPRY4 in GIST-T1/430 transfected with siRNA-SPRY4-IT1 or negative control and in GIST-T1/430 transfected with Lenti-CMV-H_SPRY4-IT1-PGK-Puro or empty vector. C. Heatmap of SPRY4 and some common genes between six high-risk GIST tissues and six low-risk GIST tissues (FC ≥ 2, P < 0.01). D. Proliferation curves of GIST-T1/430 (siRNA-SPRY4s or negative control). E. Proliferation curves of GIST-T1/430 (Lenti-CMV-H_SPRY4-PGK-Puro or empty vector). F. Colony formation graphics of GIST-T1/430 (siRNA-SPRY4s or negative control). G. Colony formation graphics of GIST-T1/430 (Lenti-CMV-H_SPRY4-IT1-PGK-Puro or empty vector). H. Expression levels of RAF1 and p-ERK (co-transfected with Lenti-CMV-H_SPRY4-PGK-Puro, Lenti-CMV-H_RAF1-PGK-Puro, or empty vector). I. Expression levels of RAF1 and p-ERK

(co-transfected with siRNA-SPRY4, siRNA-RAF1, or negative control). J. Schematic diagram of SPRY4 and SPRY4-IT1 in ERK signaling pathway. Data are displayed as the mean ± SD. *P < 0.05, **P < 0.01, ***P < 0.001. The experiments were independently repeated at least three times.

Using transcriptome sequencing, we found that miR-101-5p was manipulated by SPRY4-IT1. We also found that SPRY4-IT1 was a lncRNA localized in the cytoplasm of GIST cells and functioned as a decoy for miR-101-5p. Previous studies have reported that miR-101-5p is downregulated in several diseases and exhibits tumor-suppressive effects [25, 26]. Several other studies have identified CXCL6 as a possible target of miRNA-101-5p [27, 28]. The present study revealed the interaction between SPRY4-IT1 and miR-101-5p in GIST. The findings suggest that SPRY4-IT1 works in a protumorigenic manner in GIST by promoting cell proliferation, metastasis, and EMT. In addition, overexpression of miR-101-5p can partially rescue this effect.

Sequencing revealed that ZEB1 was modulated by miR-101-5p, which was validated by luciferase assays and miRNA pull-down analyses. In addition, miR-101-5p overexpression suppressed ZEB1 mRNA and protein expression. ZEB1 is a transcription factor that participates in EMT, which is involved in many biological processes [29-31]. Several papers have reported that ZEB1 overexpression is remarkably connected with malignancy in various cancers [30]. In the present study, we demonstrated that SPRY4-IT1 promotes GIST proliferation, metastasis, and EMT through competitively sponging miR-miR-101-5p to upregulate ZEB1 and activate the MAPK/ERK signaling pathway.

The present study also demonstrated that SPRY4-IT1 is a non-negligible lncRNA in the field of GIST tumorigenesis and progression, and it indicated that SPRY4-IT1 is associated with several tumor phenotypes, being particularly closely related to tumor risk. Thus, SPRY4-IT1 may be an important prognostic indicator for GIST in the future.

SPRY4 is considered an inhibitor of the MAPK-RAS-Raf-MEK1/2-ERK 1/2 signaling pathway [15-17, 32, 33]. However, it remains unclear whether SPRY4 is an oncogene or an oncogene suppressor remains debated [34].

SPRY4 and SPRY4-IT1 expression were highly correlated, which may be attributed to SPRY4-IT1 being an intron of SPRY4. Additionally, both SPRY4 and SPRY4-IT1 affected the phosphorylation of ERK1/ERK2 in the ERK pathway. According to the present findings, SPRY4-IT1 was found to play a dominant role between them. It is worth noting that a study on human testicular germ cell tumors has reported similar findings [34].

Acknowledgements

We would like to thank Prof. Jonathan Fletcher (Brigham and Women's Hospital, Harvard Medical School) for supplying the cell lines. This study was supported by the National Natural Science Foundation of China [NSFC-82072669 to H.C., NSFC-81702303 to L.T.] and 2017 Shanghai Outstanding Academic Leaders Plan [to H.C.].

Disclosure of conflict of interest

None.

Address correspondence to: Hui Cao and Lin Tu, Department of Gastrointestinal Surgery, Renji Hospital, School of Medicine, Shanghai Jiao Tong University, No. 1630, Dongfang Road, Shanghai 200127, P. R. China. E-mail: caohuishcn@hotmail.com (HC); tl19870228@hotmail.com (LT)

References

[1] El-Menyar A, Mekkodathil A and Al-Thani H. Diagnosis and management of gastrointestinal stromal tumors: an up-to-date literature review. J Cancer Res Ther 2017; 13: 889-900.

[2] de Pinieux G, Karanian M, Le Loarer F, Le Guellec S, Chabaud S, Terrier P, Bouvier C, Batistella M, Neuville A, Robin YM, Emile JF, Moreau A, Larousserie F, Leroux A, Stock N, Lae M, Collin F, Weinbreck N, Aubert S, Mishellany F, Charon-Barra C, Croce S, Doucet L, Quintin-Rouet I, Chateau MC, Bazille C, Valo I, Chetaille B, Ortonne N, Brouchet A, Rochaix P, Demuret A, Ghnassia JP, Mescam L, Macagno N, Birtwisle-Peyrottes I, Delfour C, Angot E, Pommepuy I, Ranchere D, Chemin-Airiau C, Jean-Denis M, Fayet Y, Courrèges JB, Mesli N, Berchoud J, Toulmonde M, Italiano A, Le Cesne A, Penel N, Ducimetiere F, Gouin F, Coindre JM and Blay JY; NetSarc/RePPS/ResSos and French Sarcoma Group- Groupe d'Etude des Tumeurs Osseuses

(GSF-GETO) networks. Nationwide incidence of sarcomas and connective tissue tumors of intermediate malignancy over four years using an expert pathology review network. PLoS One 2021; 16: e0246958.
[3] Blay JY, Kang YK, Nishida T and von Mehren M. Gastrointestinal stromal tumours. Nat Rev Dis Primers 2021; 7: 22.
[4] Ma Y, Zhang J, Wen L and Lin A. Membrane-lipid associated lncRNA: a new regulator in cancer signaling. Cancer Lett 2018; 419: 27-29.
[5] Kopp F and Mendell JT. Functional classification and experimental dissection of long noncoding RNAs. Cell 2018; 172: 393-407.
[6] Mondal T, Juvvuna PK, Kirkeby A, Mitra S, Kosalai ST, Traxler L, Hertwig F, Wernig-Zorc S, Miranda C, Deland L, Volland R, Bartenhagen C, Bartsch D, Bandaru S, Engesser A, Subhash S, Martinsson T, Caren H, Akyurek LM, Kurian L, Kanduri M, Huarte M, Kogner P, Fischer M and Kanduri C. Sense-antisense lncRNA pair encoded by locus 6p22.3 determines neuroblastoma susceptibility via the USP36-CHD7-SOX9 regulatory axis. Cancer Cell 2018; 33: 417-434, e7.
[7] Qi X, Zhang DH, Wu N, Xiao JH, Wang X and Ma W. ceRNA in cancer: possible functions and clinical implications. J Med Genet 2015; 52: 710-718.
[8] Thomson DW and Dinger ME. Endogenous microRNA sponges: evidence and controversy. Nat Rev Genet 2016; 17: 272-283.
[9] Qi M, Yu B, Yu H and Li F. Integrated analysis of a ceRNA network reveals potential prognostic lncRNAs in gastric cancer. Cancer Med 2020; 9: 1798-1817.
[10] Khaitan D, Dinger ME, Mazar J, Crawford J, Smith MA, Mattick JS and Perera RJ. The melanoma-upregulated long noncoding RNA SPRY4-IT1 modulates apoptosis and invasion. Cancer Res 2011; 71: 3852-3862.
[11] Zhao L, Jiang L, Zhang M, Zhang Q, Guan Q, Li Y, He M, Zhang J and Wei M. NF-kappaB-activated SPRY4-IT1 promotes cancer cell metastasis by downregulating TCEB1 mRNA via Staufen1-mediated mRNA decay. Oncogene 2021; 40: 4919-4929.
[12] Qie P, Yin Q, Xun X, Song Y, Zhou S, Liu H, Feng J and Tian Z. Long non-coding RNA SPRY4-IT1 as a promising indicator for three field lymph-node dissection of thoracic esophageal carcinoma. J Cardiothorac Surg 2021; 16: 48.
[13] Cao S, Lin L, Xia X and Wu H. lncRNA SPRY4-IT1 regulates cell proliferation and migration by sponging miR-101-3p and regulating AMPK expression in gastric cancer. Mol Ther Nucleic Acids 2019; 17: 455-464.
[14] Ma W, Chen X, Wu X, Li J, Mei C, Jing W, Teng L, Tu H, Jiang X, Wang G, Chen Y, Wang K, Wang H, Wei Y, Liu Z and Yuan Y. Long noncoding RNA SPRY4-IT1 promotes proliferation and metastasis of hepatocellular carcinoma via mediating TNF signaling pathway. J Cell Physiol 2020; 235: 7849-7862.
[15] Leeksma OC, Van Achterberg TA, Tsumura Y, Toshima J, Eldering E, Kroes WG, Mellink C, Spaargaren M, Mizuno K, Pannekoek H and de Vries CJ. Human sprouty 4, a new ras antagonist on 5q31, interacts with the dual specificity kinase TESK1. Eur J Biochem 2002; 269: 2546-2556.
[16] Guo J, Zhu H, Li Q, Dong J, Xiong W and Yu K. SPRY4 suppresses proliferation and induces apoptosis of colorectal cancer cells by repressing oncogene EZH2. Aging (Albany NY) 2021; 13: 11665-11677.
[17] Park S, Arai Y, Kim BJ, Bello A, Ashraf S, Park H, Park KS and Lee SH. Suppression of SPRY4 promotes osteogenic differentiation and bone formation of mesenchymal stem cell. Tissue Eng Part A 2019; 25: 1646-1657.
[18] Yuan J, Dong X, Yap J and Hu J. The MAPK and AMPK signalings: interplay and implication in targeted cancer therapy. J Hematol Oncol 2020; 13: 113.
[19] Sheng W, Shi X, Lin Y, Tang J, Jia C, Cao R, Sun J, Wang G, Zhou L and Dong M. Correction to: Musashi2 promotes EGF-induced EMT in pancreatic cancer via ZEB1-ERK/MAPK signaling. J Exp Clin Cancer Res 2020; 39: 167.
[20] Hu Q, Ma X, Li C, Zhou C, Chen J and Gu X. Downregulation of THRSP promotes hepatocellular carcinoma progression by triggering ZEB1 transcription in an ERK-dependent manner. J Cancer 2021; 12: 4247-4256.
[21] Li YH, Hu YQ, Wang SC, Li Y and Chen DM. LncRNA SNHG5: a new budding star in human cancers. Gene 2020; 749: 144724.
[22] Ma B, Li Y and Ren Y. Identification of a 6-lncRNA prognostic signature based on microarray re-annotation in gastric cancer. Cancer Med 2020; 9: 335-349.
[23] Long J, Bai Y, Yang X, Lin J, Yang X, Wang D, He L, Zheng Y and Zhao H. Construction and comprehensive analysis of a ceRNA network to reveal potential prognostic biomarkers for hepatocellular carcinoma. Cancer Cell Int 2019; 19: 90.
[24] Zhang K, Zhang L, Mi Y, Tang Y, Ren F, Liu B, Zhang Y and Zheng P. A ceRNA network and a potential regulatory axis in gastric cancer with different degrees of immune cell infiltration. Cancer Sci 2020; 111: 4041-4050.
[25] Toda H, Seki N, Kurozumi S, Shinden Y, Yamada Y, Nohata N, Moriya S, Idichi T, Maemura K, Fujii T, Horiguchi J, Kijima Y and Natsugoe S.

RNA-sequence-based microRNA expression signature in breast cancer: tumor-suppressive miR-101-5p regulates molecular pathogenesis. Mol Oncol 2020; 14: 426-446.
[26] Yamada Y, Nohata N, Uchida A, Kato M, Arai T, Moriya S, Mizuno K, Kojima S, Yamazaki K, Naya Y, Ichikawa T and Seki N. Replisome genes regulation by antitumor miR-101-5p in clear cell renal cell carcinoma. Cancer Sci 2020; 111: 1392-1406.
[27] Shen W, Xie XY, Liu MR and Wang LL. MicroRNA-101-5p inhibits the growth and metastasis of cervical cancer cell by inhibiting CXCL6. Eur Rev Med Pharmacol Sci 2019; 23: 1957-1968.
[28] Chen Q, Liu D, Hu Z, Luo C and Zheng SL. miRNA-101-5p inhibits the growth and aggressiveness of NSCLC cells through targeting CXCL6. Onco Targets Ther 2019; 12: 835-848.
[29] Cheng L, Zhou MY, Gu YJ, Chen L and Wang Y. ZEB1: new advances in fibrosis and cancer. Mol Cell Biochem 2021; 476: 1643-1650.
[30] Zhang Y, Xu L, Li A and Han X. The roles of ZEB1 in tumorigenic progression and epigenetic modifications. Biomed Pharmacother 2019; 110: 400-408.
[31] Larsen JE, Nathan V, Osborne JK, Farrow RK, Deb D, Sullivan JP, Dospoy PD, Augustyn A, Hight SK, Sato M, Girard L, Behrens C, Wistuba II, Gazdar AF, Hayward NK and Minna JD. ZEB1 drives epithelial-to-mesenchymal transition in lung cancer. J Clin Invest 2016; 126: 3219-3235.
[32] Sasaki A, Taketomi T, Kato R, Saeki K, Nonami A, Sasaki M, Kuriyama M, Saito N, Shibuya M and Yoshimura A. Mammalian Sprouty4 suppresses Ras-independent ERK activation by binding to Raf1. Nat Cell Biol 2003; 5: 427-432.
[33] Li J, Li N, Chen Y, Hui S, Fan J, Ye B, Fan Z, Zhang J, Zhao RC and Zhuang Q. SPRY4 is responsible for pathogenesis of adolescent idiopathic scoliosis by contributing to osteogenic differentiation and melatonin response of bone marrow-derived mesenchymal stem cells. Cell Death Dis 2019; 10: 805.
[34] Das MK, Furu K, Evensen HF, Haugen OP and Haugen TB. Knockdown of SPRY4 and SPRY4-IT1 inhibits cell growth and phosphorylation of Akt in human testicular germ cell tumours. Sci Rep 2018; 8: 2462.

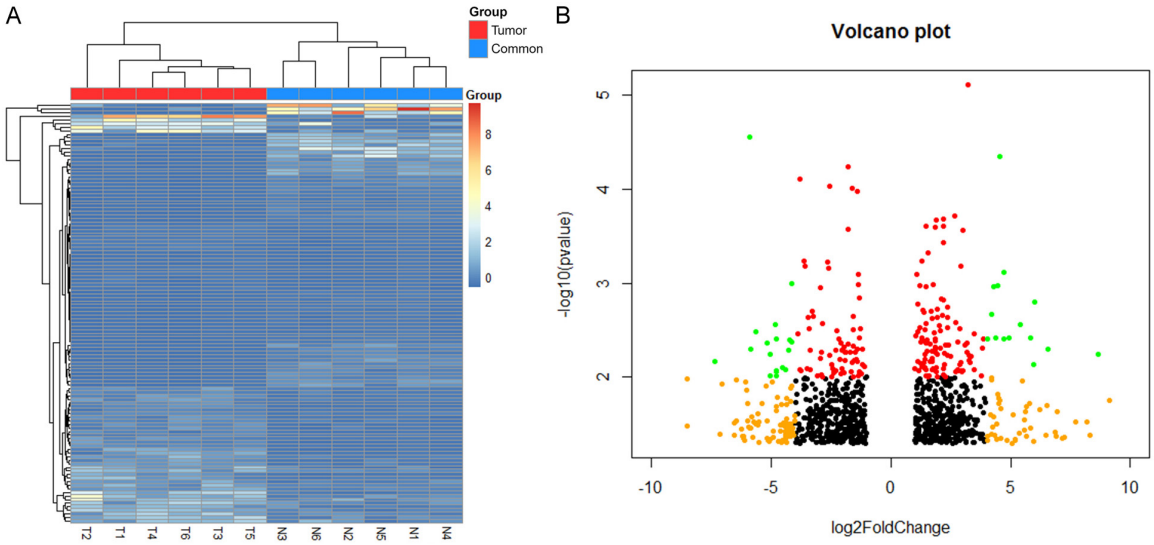

Figure S1. LncRNA SPRY4-IT1 is overexpressed in high-risk GIST. (A, B) Hierarchical clustering diagram (Heatmap) and (A) Volcano Plot (B) illustrating the differentially expressed lncRNAs between six high-risk GIST tissues and six low-risk GIST tissues (fold change ≥ 4, P < 0.01).

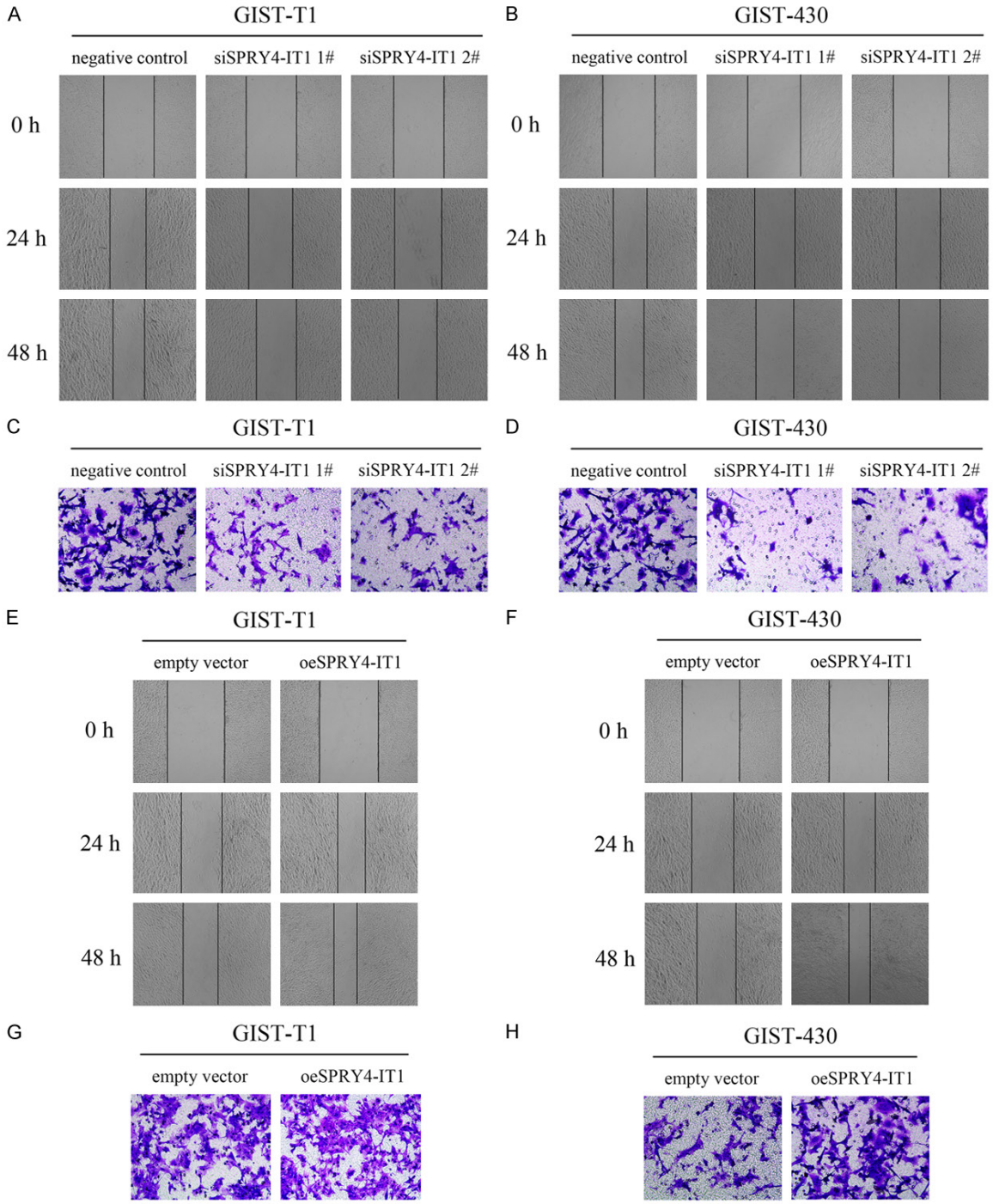

Figure S2. SPRY4-IT1 promotes GIST cell migration. (A, B) Wound healing assays in GIST-T1 (A)/GIST-430 (B) transfected with siRNA-SPRY4-IT1s or negative control. (C, D) Transwell migration assays of GIST-T1 (C)/GIST-430 (D) transfected with siRNA-SPRY4-IT1s or negative control. (E, F) Wound healing assays of GIST-T1 (E)/GIST-430 (F) transfected with Lenti-CMV-H_SPRY4-IT1-PGK-Puro or empty vector. (G, H) Transwell migration assays of GIST-T1 (G)/GIST-430 (H) transfected with Lenti-CMV-H_SPRY4-IT1-PGK-Puro or empty vector.

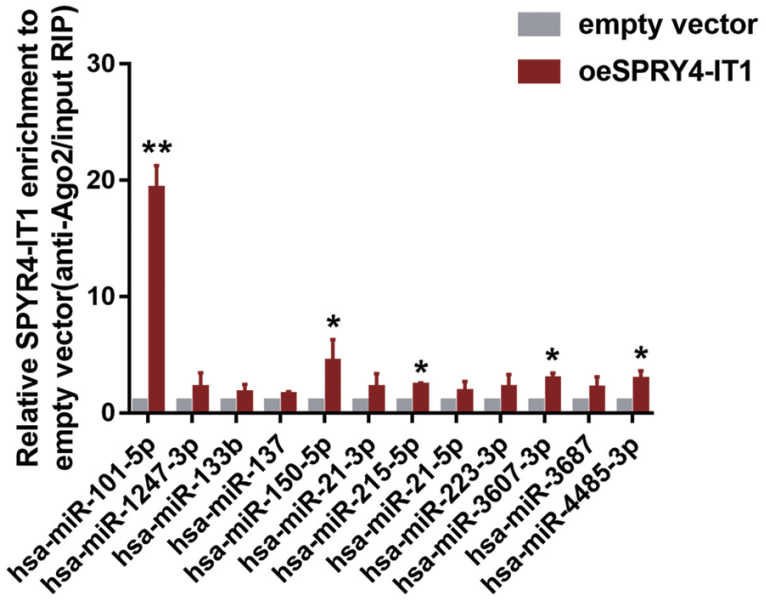

Figure S3. SPRY4-IT1 acts as a ceRNA for miR-101-5p. Top 12 predicted miRNAs in GIST-T1 transfected with Lenti-CMV-H_SPRY4-IT1-PGK-Puro or empty vector by Ago2-RIP.

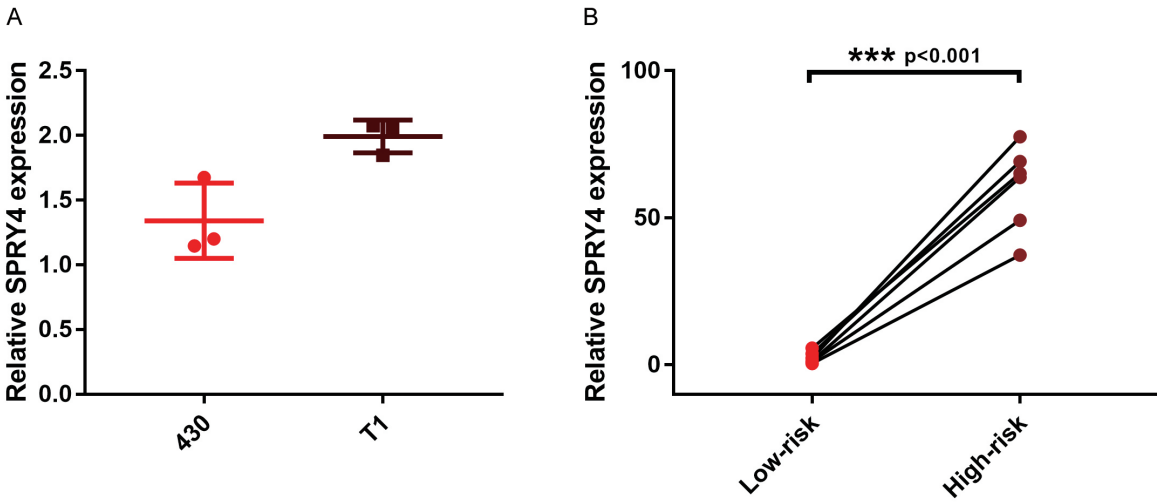

C

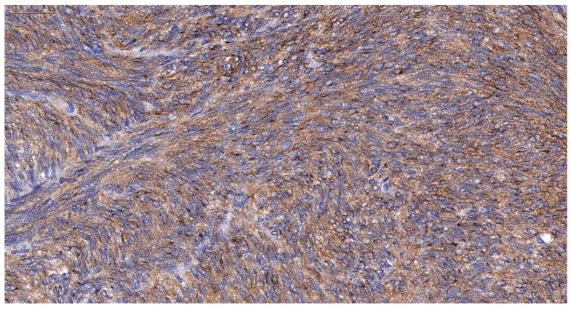

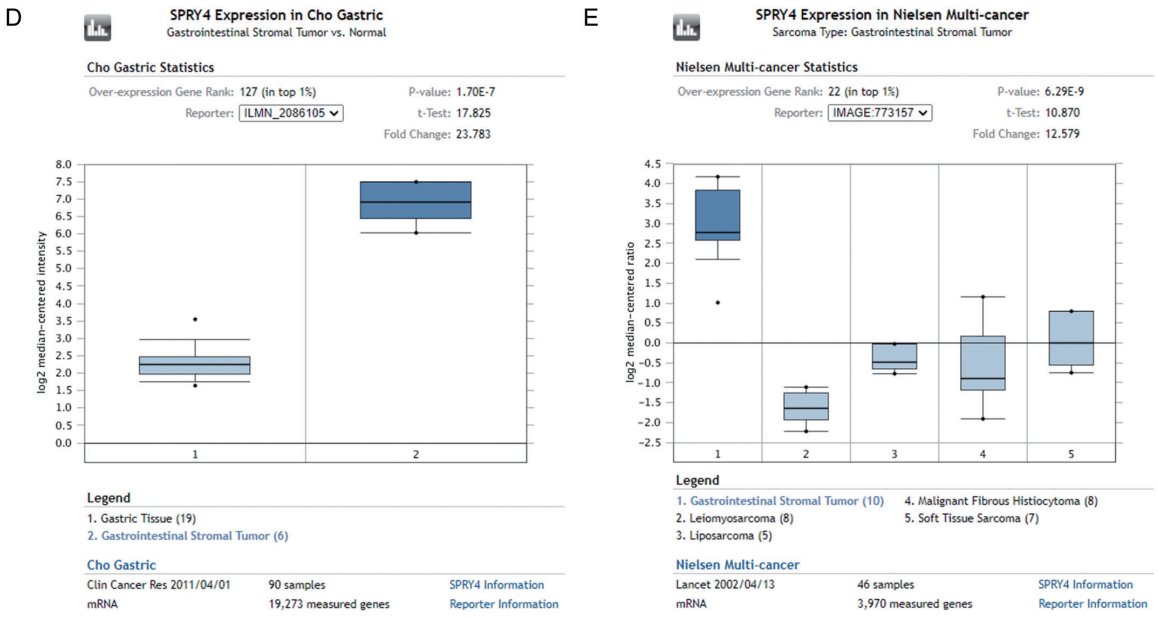

Figure S4. SPRY4 is overexpressed in high-risk GIST. A. SPRY4 expression level in the GIST-T1/430. B. SPRY4-IT1 expression in GIST tissues (low-risk n = 6, high-risk n = 6). C. SPRY4 expression in high-risk GIST tissues detected using immunohistochemistry. D. SPRY4 expression in tissues (gastric tissues n = 6, GIST tissues n = 6) identified using an online database (Oncomine). E. SPRY4 expression in tissues of GIST and other sarcomas identified using an online database (Oncomine).

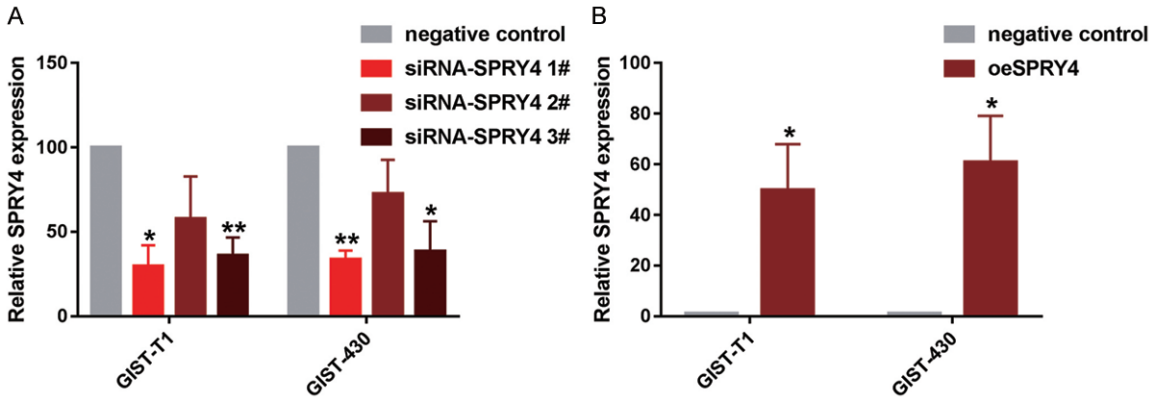

Figure S5. Validation of SPRY4 knockdown and overexpression. (A, B) Expression of SPRY4 in GIST-T1/430 (siRNA-SPRY4s or negative control) (A) and in GIST-T1/430 (Lenti-CMV-H_SPRY4-PGK-Puro or empty vector) (B).